# A Focused Chromium Ion Beam

Running Title: A Focused Chromium Ion Beam

Running Authors: Steele, Knuffman, McClelland and Orloff

A.V. Steele, B. Knuffman, J.J. McClelland

Center for Nanoscale Science and Technology, National Institute of Standards and Technology, Gaithersburg, MD

J. Orloff

FEI Company, Hillsboro, OR

## I. Abstract

With the goal of expanding the capabilities of focused ion beam microscopy and milling systems, we have demonstrated nanoscale focusing of chromium ions produced in a magneto-optical trap ion source (MOTIS). Neutral chromium atoms are captured into a magneto-optical trap and cooled to 100 μK with laser light at 425 nm. The atoms are subsequently photoionized and accelerated to energies between 0.5 keV and 3 keV. The accelerated ion beam is scanned with a dipolar deflector and focused onto a sample by an einzel lens. Secondary electron images are collected and analyzed, and from these a beam diameter is inferred. The result is a focused probe with a one-standard-deviation radius as small as 205±10 nm. While this probe size is in the useful range for nanoscale applications, it is almost three times larger than is predicted by ray-tracing simulations. Possible explanations for this discrepancy are discussed.

## II.

Focused ion beams (FIBs) are a proven tool for surface interrogation and modification at the nanoscale. The most common uses of FIB technology are in milling[1], microscopy[2], and ion implantation[3]. In each of these applications, inherent properties of the ion source impose limits

on the ability to perform tasks with high resolution, with a desired level of selectivity, and with sufficient speed. The ultimate resolution of a FIB device depends primarily on the ion source brightness, emittance and energy spread. The most widely used ion source, the liquid metal ion source (LMIS), is also practically limited to a few atomic species, primarily gallium. Alloys may be employed to broaden the species selection somewhat, but to achieve a monatomic beam then requires a mass selection filter[4]. Gas-phase ion sources are also available, but long lifetime, high-brightness operation has been elusive in species besides helium[5].

In this report, we demonstrate progress towards the implementation of a magneto-optical trap ion source[6,7] (MOTIS) -based chromium FIB. Additionally, for the first time, we present images created using an ultra-cold ion source. Previously, a number of schemes for the creation of two-dimensionally-cooled ions[8] and magneto-optical-trap-extracted electrons[9] were proposed. Subsequently, the MOTIS emittance was directly measured[10], as was the energy spread for ions extracted from a similar apparatus[11].

Investigations so far suggest the great potential of ultra-cold gases to address numerous FIB applications, while advancing the state of the art along a number of the dimensions used as metrics for FIB performance: emittance, brightness, beam energy spread and the variety of atomic species available. Additionally, a MOTIS can provide capabilities, such as deterministic single ion delivery[12,13], that more conventional ion sources could not hope to achieve. Figure 1 shows the large and growing number of atoms that can be laser cooled. The applicability of the MOTIS technique to any of these atoms opens up a number of possibilities for new experiments. The nanoscopic, variable energy, isotopically pure surface probe provided by a MOTIS-based FIB could be invaluable for the study of surface chemistry[14] and nanoscale device fabrication. As just one example, a chromium focused ion beam would permit the precise placement of single-photon color-centers in bulk diamond[15].

In any ion beam system, emittance is a figure of critical importance for the assessment of beam quality. While there is no single accepted definition for this quantity, most definitions convey something about the beam's moments in phase or trace space[16]. We use a trace-space rms emittance normalized by the beam's energy

$$\varepsilon_{rms} = \sqrt{\left\langle x^2 \right\rangle \left\langle x'^2 \right\rangle - \left\langle xx' \right\rangle^2}\sqrt{U}, \qquad (1)$$

where $x$ is the transverse coordinate, $x'$ is the transverse angle, and $U$ is the beam energy. This emittance is a conserved quantity through an ion-optical system, including beam lines with acceleration or focusing, but neglecting those with beam aperturing, aberrations or Coulomb effects. This makes it a convenient quantity for calculating the spot size that is achievable given a particular source. To achieve a low emittance in a collimated beam, the trace-space area must be minimized. In a MOTIS, the angular spread is set by the temperature of the ions in the source, and the spatial extent is set by the size of the ionization region. This implies the best MOTIS performance will be obtained with lower temperatures and ionization regions with small cross-sections along the beam's propagation axis. In earlier work an emittance measurement for the chromium MOTIS yielded the value $6.0\times10^{-7}$ mm mrad $\sqrt{\text{MeV}}$ [10]. This number compares favorably with a typical value for the LMIS of $1.1\times10^{-6}$ mm mrad $\sqrt{\text{MeV}}$ in high-resolution mode.

For FIB applications where images must be collected rapidly, where significant aperturing is required, or where the surface ion dose is of paramount importance, the beam brightness is a more useful metric of ion source performance. The brightness may be written

$$B = \frac{\partial^2 I}{\partial A \partial \Omega U} = \frac{I}{8\pi^2 \varepsilon_{rms,x} \varepsilon_{rms,y}}, \qquad (2)$$

where $I$ is the beam current, $A$ is the beam's cross-sectional area, and $\Omega$ the solid angle. It is an invariant along the beam line when $\varepsilon_{rms}$ is invariant and the current is constant. However, brightness is also conserved through a beam aperture for some current density distributions, though this is not strictly the case in the Gaussian current distribution provided by the MOTIS. In SI units, the LMIS brightness[17-19] is between ($10^5$ and $10^6$) $\text{Am}^{-2}\text{sr}^{-1}\text{eV}^{-1}$. In more convenient units, this brightness can be expressed as being between ($10^{-4}$ and $10^{-3}$) pA $\text{nm}^{-2}$ $\mu\text{sr}^{-1}$ $\text{keV}^{-1}$. Noting that convergence angles in the final lens of most FIBs are about 1 mrad ($\pi$ mrad$^2$=1 $\mu$sr) and the most ion beam energies are in the kilo electron volt range, these brightness units rapidly give an idea of the current an ion beam can deliver into a nano-scale region of a target's surface.

In the MOTIS, there are a number of mechanisms that limit the brightness. The rate of diffusion of cold, trapped atoms from the body of the magneto-optical trap (MOT) into the small ionization region sets one upper limit on the current that can be extracted [20]. Additionally, the rate at which hot neutral atoms can be captured from the atomic beam into the MOT imposes an

upper bound of 160 pA or more[21] on the total current that could be available for extraction[7]. A brightness of up to $4.9\times10^{-5}$ pA nm$^{-2}$ μsr$^{-1}$ keV$^{-1}$ has been achieved in the chromium MOTIS, though the measurements reported here were performed with a somewhat lower brightness of $8.8\times10^{-6}$ pA nm$^{-2}$ μsr$^{-1}$ keV$^{-1}$. It is important to note that these numbers are not indicative of a fundamental limit to the MOTIS brightness but rather they represent the brightness seen in a first-generation, non-optimized system. In practice, numerous techniques commonly used in atom trapping experiments, such as atomic beam collimation[21] and Zeeman slowing[22] may be employed to obtain a source brightness at least a factor of ten larger than our present value for a chromium beam and significantly higher for many other atomic species.

While emittance dictates how tightly a beam may be focused, if a beam is not mono-energetic, chromatic aberrations can also contribute to an increased focal spot size. In a LMIS, the created ions have an energy spread of a few electron volts, believed to be due to Coulomb effects near the ions' point of creation[17]. Chromatic aberrations resulting from this energy spread are usually what limit LMIS FIB resolution and are one of the main reasons LMIS FIBs are operated in the 30 keV range.

In the MOTIS, inherent energy spread from the temperature of the ions is completely negligible (of order 10 neV for 100 μK). However, chromatic spread does arise from the spatial extent of the ion source along the beam axis, since the atoms are ionized in an electric field (i.e., a potential with a gradient). If the spatial extent of the ionization region has a one-standard-deviation width of $\sigma_{ion}$, then the one-standard-deviation energy spread of the beam can be written as

$$\sigma_U = e\sigma_{ion}E, \quad (3)$$

where *e* is the ion charge and *E* is the local electric field. The spatial extent of the ionization region $\sigma_{ion}$ can take two different forms, depending on how the ionization laser intersects the MOT. If it is incident perpendicular to the ion beam axis (transverse, or radial ionization), $\sigma_{ion}$ will be equal to $\sigma_{laser}$, the one-standard-deviation radius of the ionization laser beam. If, on the other hand, it is incident along the ion beam axis (axial ionization), $\sigma_{ion}$ will be equal to $\sigma_{MOT}$, the one-standard-deviation radius of the cloud of cold atoms in the MOT.

Each of these two ionization geometries has its own relative advantages and disadvantages. Transverse ionization allows one to minimize the energy spread by focusing the ionization laser into a very narrow beam. In this case the laser beam waist can be reduced to very small values, limited only by reaching the point where the rate of diffusion into the ionization region begins to limit the extractable beam current. This rate depends strongly on the particular atom being cooled, but we have seen, for example, that for chromium the beam waist can be reduced to 10 μm before any reduction in beam current is observed. However, transverse ionization generally results in less ion current since an aperture will often be needed to avoid spherical and chromatic aberrations in the final lens. Axial ionization, on the other hand, provides significantly more current in a symmetric beam because it does not require an aperture. Changing the ionization laser beam waist in this case changes the source emittance but does not affect the energy spread. The energy spread is, however, significantly larger for axial ionization because the ions are created over a much larger region, typically several hundred micrometers in size. For example with the acceleration geometry of the present setup and $\sigma_{MOT} \approx 50$ μm, a 3 keV beam would have a $\sigma_U$ of 0.6 eV.

An important difference between the MOTIS and the LMIS is the level of control that exists over the energy spread. Whereas the LMIS energy spread is fixed, the MOTIS spread can be adjusted not only by changing the ionization mode and laser beam size, but also by choosing the magnitude of the extraction electric field. While this affords some degree of freedom, it must be borne in mind that the extraction field also plays a significant role in determining the ion optical behavior of the source. If too small an extraction field is used, it becomes difficult to accelerate the ions to a high energy without using long acceleration distances or else incurring strong focusing effects.

A schematic of the ion creation and acceleration regions of our apparatus is shown in Fig. 2, and the relevant energy levels in Cr for cooling and photoionization are shown in Fig. 3. Neutral Cr atoms are captured and cooled from an atomic beam into the MOT[23]. The MOT is created by the intersection of six laser beams and the zero of a quadrupolar magnetic field formed by a pair of oppositely oriented ring shaped strong permanent NdFeB magnets. These magnets have an outer diameter of 75 mm and an inner diameter of 38 mm, a thickness of 25 mm and a $B_r$=1.3 T. When spaced by 215 mm these magnets produce gradients of 0.16 T $m^{-1}$ along

the magnetization axis and 0.08 T $m^{-1}$ in the plane perpendicular to this axis. The laser light is created by second harmonic generation of the output of a Ti:Sapphire laser, which is in turn pumped by a diode pumped solid-state laser. A few mW in each of the 6 laser beams, which nominally have a $1/e^2$ diameter of 4 mm, is sufficient to create the atom trap. The laser beams are tuned just below the Cr $^7S_3 \rightarrow {}^7P_4$ transition at 425 nm. The trapped cold atom ensemble is generally spherically symmetric and has an approximately Gaussian density profile with a standard deviation radius ranging from 50 μm to 100 μm, depending on laser beam intensity, detuning and alignment. We measured the temperature of the trapped atoms by turning off the laser light and allowing the atoms to freely expand for a time. The temperature inferred from the rate of expansion of the atomic distribution was 100±15 μK[1]. The ionization laser is focused through the MOT along the ion beam axis (axial ionization) and has an essentially Gaussian beam waist of standard deviation 5 μm ($1/e^2$ diameter of 20 μm).

The ions are extracted in an electric field created by two parallel plates separated by 15 mm, one consisting of a fused silica window with a transparent, conducting, indium tin oxide(ITO) coating, and the other a reflecting aluminum-coated 100 μm thick silicon electrode with a 4 mm diameter hole at the center through which the ions pass. The ions are accelerated to their final energy in a 265 mm long tube made of resistive glass, the beginning of which is 0.4 mm behind the silicon electrode, and the far end of which is grounded. Voltages on the ITO-coated and aluminum-coated electrodes are chosen such that the electric field between the plates is equal to the uniform electric field in the resistive tube. Because the fields in these two regions are equal, and because the distance between the reflecting aluminum electrode and the start of the resistive tube is small, there is essentially no lensing as the ions pass from the region between the plates into the resistive tube. The ions do however experience a relatively weak diverging lens as they exit the resistive tube. In our system the free flight distance between the tube exit and the focusing optics is less than 100 mm. Therefore, the ion beam diameter at the focusing lens should be very close to that of the source width, which was typically set to 10μm.

The focusing optics are composed of three parts: a two-axis dipolar deflector, a three-element einzel lens, and a channel-electron multiplier for secondary electron detection. A

[1] Unless otherwise specified, all uncertainties in this paper are intended to be interpreted as one-standard-deviation, combined standard uncertainty.

drawing of these elements is shown in Fig. 4. There are no beam limiting apertures in any of these optics. The deflector plate voltage is supplied by a fast amplifier with a range of 100 V and a settling time of 50 μs. The voltage range on the amplifier permits beam deflections from a few nanometers up to a few millimeters. Ions were either projected onto a micro-channel plate and phosphor screen at a working distance, defined as the distance from the closest surface of the lens to the target, of 28 mm, or onto a sample stage mounted at a working distance of 17 mm. Secondary ion counts from these targets were up to $2\times10^5$ $s^{-1}$ for a 0.2 pA ion beam.

An image formed using this apparatus is shown in Fig. 5. The sample in this case is a piece of a microchannel plate mounted at a working distance of 17 mm. The 10 μm pores in the plate are clearly resolved, showing good resolution and contrast in this first-ever image taken with a Cr focused ion beam.

To determine the probe size of the focused ion beam we analyzed a series of images similar to Fig. 5 taken at a working distance of 28 mm, using the microchannel plate of our beam imager as a target. We note that images taken at 17 mm and 28 mm working distance did not show significant differences in image quality. Our analysis was performed with the assumption that the focused beam's current density distribution was Gaussian, which is expected because the distribution is inherited from the ionization laser intensity distribution, with only small distortions caused by lens aberrations. The standard deviation of this distribution was obtained from error function fits to the secondary electron counts as the beam was swept from a dark to a light area of the image. Calibration of the scans was obtained from the 10 μm diameter of the microchannel plate pores.

Observed Gaussian beam widths as a function of beam energy are shown in Fig. 6. The smallest beam size we observed was 205±10 nm at 3 keV energy. A clear increase in beam size is seen with decreasing energy, with the one-standard-deviation width reaching 318±16 nm at 0.5 keV energy.

With the goal of improving our understanding of the performance of our focused Cr beam MOTIS realization, we conducted simulations using commercial ray-tracing software, using an initial ion temperature and spatial extent consistent with measurements of our source parameters. Surprisingly, these calculations predicted current distribution standard deviations of approximately 70 nm, about a factor of three smaller than our observed widths. A number of

possibilities present themselves as explanations for this discrepancy. First, it is possible that numerical accuracy in the calculations is not as high as it should be. Work is currently underway to test this hypothesis. Second, machining tolerances and imperfect alignment of the ion optics could cause a larger spot size. The optics were constructed without extraordinary precision beyond standard machine tolerances of several tens of micrometers, and preliminary estimates of astigmatism and coma arising from such tolerances yield blurs that are in the range of what we observe. Third, inter-ion Coulomb forces[20] could be causing an increase in the transverse temperature of the ion beam, and hence an increased emittance. With the extremely low current density of $2.5 \times 10^{-3}$ A $m^{-2}$ along the whole ion beam, except at the focus, this does not seem likely. However, the energy of the beam is low for an extended length of time during acceleration in the resistive tube, which could exacerbate space charge effects. Furthermore, preliminary Monte Carlo calculations suggest there may be some Coulomb effect. Fourth, the experimental apparatus could be subject to relative mechanical vibrations of the sample and ion optics, causing a smearing of the image. This potential cause is also the subject of ongoing diagnostic experiments.

Regarding mechanical vibrations, it is worth noting that the MOTIS should be far less susceptible to source vibrations than most other ion sources. In most FIBs, where a real source is being imaged onto a target with only a modest (if any) demagnification, any vibrations of the source will be reflected in vibrations of the beam in the image plane. Since in the MOTIS the ions are created in a collimated beam and the probe-forming optics image a virtual source at very high demagnification, any spatial vibrations of the ion production region should be greatly reduced in the image plane. We tested this property of the source by modulating the position of the ionization laser in the MOT at 1 kHz and looking for a change in image quality. No change was observed, even for beam deviations of 50 μm, which is of the same order as the MOT size.

We have presented our progress towards producing a focused chromium ion beam using ions from a MOTIS. Cold chromium atoms were ionized and extracted from a MOT, accelerated to energies between 0.5 keV and 3 keV and focused onto a target. Secondary electrons were collected to create an image. The smallest beam diameter at the target was found to be 205±10 nm at 3 keV beam energy. This is approximately three times larger than predicted by simulations. Cold ions are a promising alternative to conventional liquid metal or gas-phase ion sources due to their low emittance and potentially high brightness, combined with the

technique's amenability to a wider selection of atomic species. Much work in characterizing these sources remains to be done before their ultimate performance can be realized.

## Acknowledgment.

The authors would like to thank D. Rutter and A. Band for the construction of the deflector amplifier.

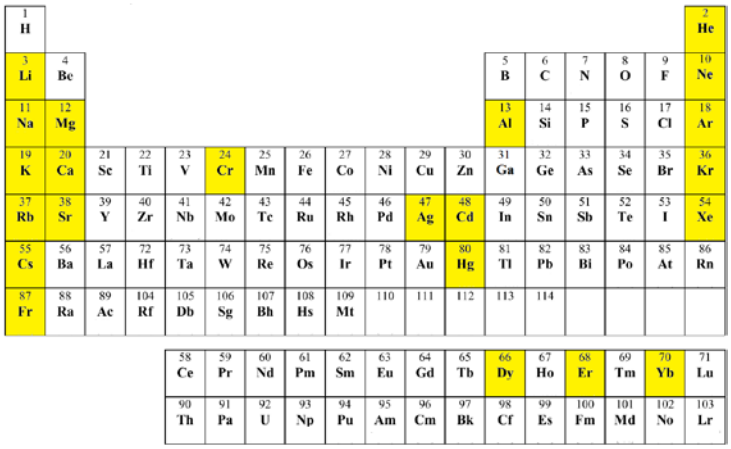


FIG 1

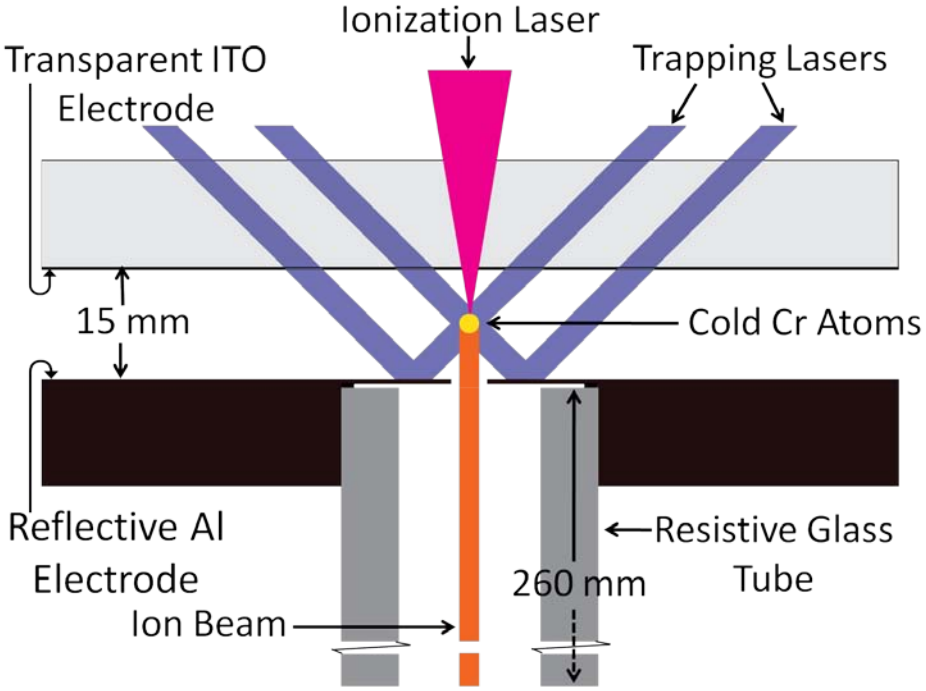
Ionization Laser
Transparent ITO
Electrode
Trapping Lasers
15 mm
Cold Cr Atoms
Reflective Al
Electrode
Resistive Glass
Tube
260 mm
Ion Beam

FIG 2

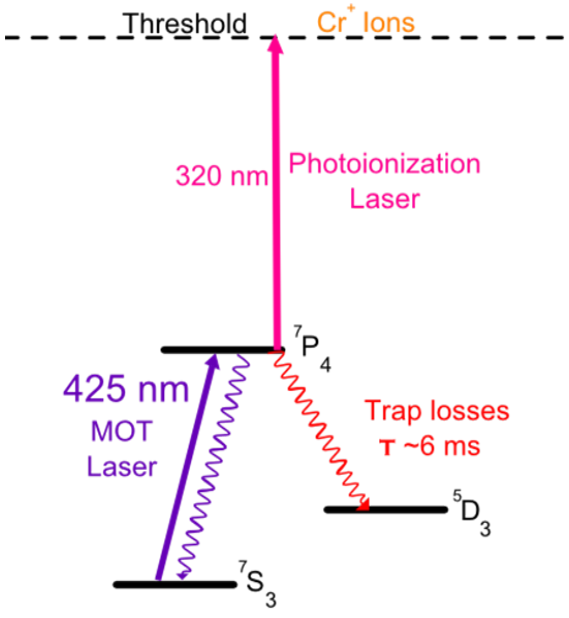
Threshold
Cr+ Ions
320 nm
Photoionization
Laser
7P4
425 nm
MOT
Laser
Trap losses
τ ~6 ms
5D3
7S3

FIG 3

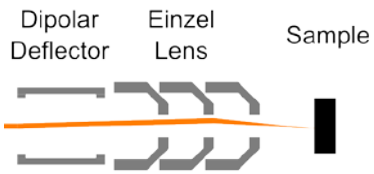


FIG 4

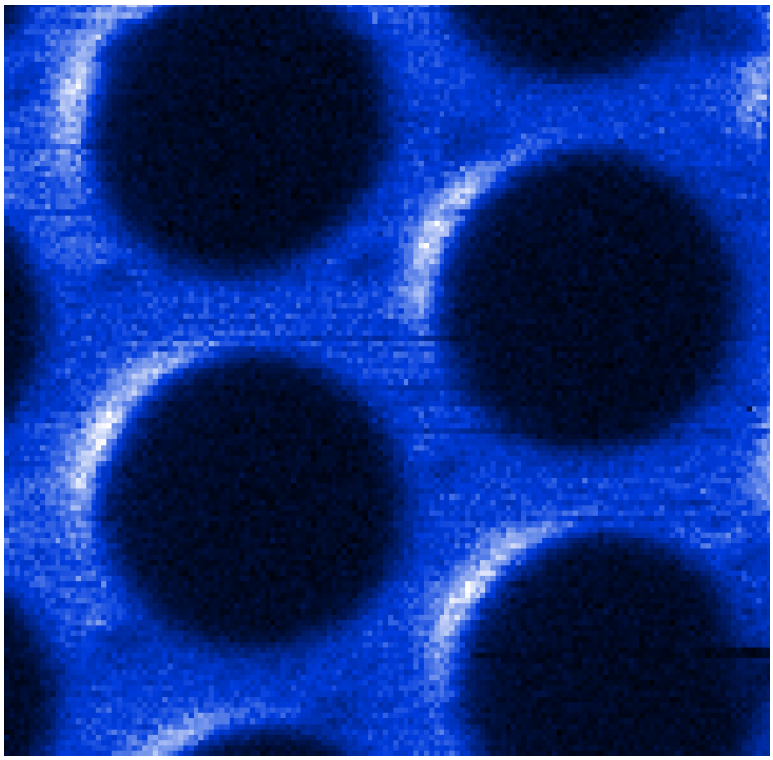

FIG 5

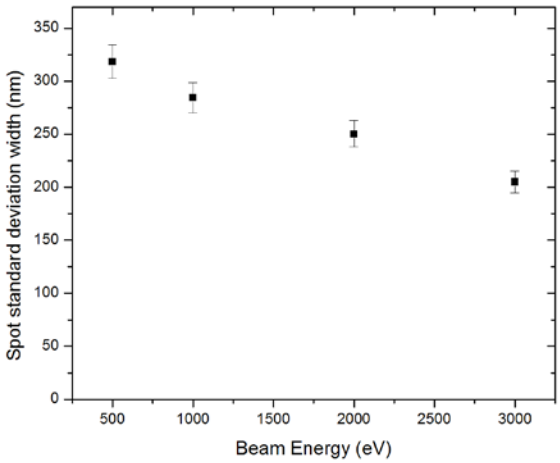
Spot standard deviation width (nm)
350
300
250
200
150
100
50
0
500
1000
1500
2000
2500
3000
Beam Energy (eV)

FIG 6

FIG 1. Current state of MOTIS-compatible atomic species. Elements in which laser cooling has been demonstrated are marked. As laser technology advances, it is expected that more elements will become available.

FIG 2. Ion source cross-section. Two pairs of counter-propagating laser beams pass through a transparent electrode and are reflected by a mirror electrode. The spacing between these electrodes is 15 mm. At the intersection of these four beams another beam pair runs perpendicular to the figure. This intersection is half way between the two electrodes. The permanent magnets also lie along the axis out of the page. Photoionized atoms extracted from the MOT are accelerated through a 4 mm diameter hole in the mirror electrode. The ions are then accelerated by a constant electric-field over the length of a 265 mm long tube made of resistive glass. Typically, the electric field in the tube is matched to that between the two other electrodes, ensuring that there is no focusing of the ions as they are accelerated.

FIG. 3 Pertinent energy levels in neutral chromium. Laser cooling and trapping is provided by light at 425 nm. Losses from the excited $^7P_4$ state limit the trap lifetime to 6 ms. Ionization of trapped atoms is performed by excitation at 320 nm from the excited state to just above threshold.

FIG 4. Ion focusing optics. The dipolar deflector is composed of two pairs of plates 25 mm long and separated by 10 mm. The einzel lens is made from a set of 3 axially symmetric semi-conical elements with thickness 1.5 mm, spacing 20 mm and a clear aperture of 3 mm.

FIG 5. FIB secondary electron image. The target is a piece of a micro-channel plate with 10 μm pores. The beam energy is 2 kV and the beam size is 250 nm. This image is 300x300 pixels and took 90 s to acquire.

FIG 6. Measured beam spot standard deviation radius versus beam energy between 0.5 and 3 keV.

Reference List


[1] J.Orloff, L.Swanson, and M.W.Utlaut, *High Resolution Focused Ion Beams*, (Kluwer Academic/Plenum Publishers, New York, 2003).

[2] M. T. Postek and A. E. Vladar, Scanning **30**(6), 457 (2008).

[3] A. Shahmoon, O. Limon, O. Girshevitz, Y. Fleger, H. V. Demir, and Z. Zalevsky, Microelectronic Engineering **87**(5-8), 1363 (2010).

[4] L. Bischoff, Ultramicroscopy **103**(1), 59 (2005).

[5] J. Notte, FHM Rahman, SM McVey, S Tan, and R Livengood, Microscopy and Microanalysis **16**(S2), 28 (2010).

[6] J. L. Hanssen, E. A. Dakin, J. J. McClelland, and M. Jacka, J. Vac. Sci. Technol. B. **24**(6), 2907 (2006).

[7] J. L. Hanssen, J. J. McClelland, E. A. Dakin, and M. Jacka, Phys. Rev. A. **74**(6), 063416 (2006).

[8] B. G. Freinkman, A. Eletskii, and S. I. Zaitsev, Microelectronic Engineering **73-74**, 139 (2004).

[9] B. J. Claessens, S. B. Van Der Geer, G. Taban, E. J. D. Vredenbregt, and O. J. Luiten, Phys. Rev. Lett. **95**(16), 164801 (2005).

[10] J. L. Hanssen, S. B. Hill, J. Orloff, and J. J. McClelland, Nano. Lett. **8**(9), 2844 (2008).

[11] M. P. Reijnders, P. A. van Kruisbergen, G. Taban, S. B. Van Der Geer, P. H. A. Mutsaers, E. J. D. Vredenbregt, and O. J. Luiten, Phys. Rev. Lett. **102**(3), 034802 (2009).

[12] S. B. Hill and J. J. McClelland, Appl. Phys. Lett. **82**(18), 3128 (2003).

[13] S. B. Hill and J. J. McClelland, J. Opt. Soc. Am. B. **21**(3), 473 (2004).

[14] V. Grill, J. Shen, C. Evans, and R. G. Cooks, Rev. Sci. Inst. **72**(8), 3149 (2001).

[15] I. Aharonovich, S. Castelletto, B. C. Johnson, J. C. McCallum, D. A. Simpson, A. D. Greentree, and S. Prawer, Phys. Rev. B. **81**(12) (2010).

[16] M.Reiser, *Theory and Design of Charged Particle Beams*, (Wiley-VCH, Weinheim, 2008).

[17] G. D. Alton and P. M. Read, J. Appl. Phys. **66**(3), 1018 (1989).

[18] R. L. Seliger, J. W. Ward, V. Wang, and R. L. Kubena, Appl. Phys. Lett. **34**(5), 310 (1979).

[19] D. Loffelmacher, J. Adamczewski, A. Stephan, J. Meijer, H. Rocken, H. H. Bukow, and C. Rolfs, Nucl. Instr. and Meth. in Phys. Res. B. **139**(1-4), 422 (1998).

[20] S. B. Van Der Geer, M. P. Reijnders, M. J. de Loos, E. J. D. Vredenbregt, P. H. A. Mutsaers, and O. J. Luiten, J. Appl. Phys. **102**(9), 094312 (2007).

[21] C. Slowe, L. Vernac, and L. V. Hau, Rev. Sci. Inst. **76**(10), 103101 (2005).

[22] W. D. Phillips and H. Metcalf, Phys. Rev. Lett. **48**(9), 596 (1982).

[23] E. L. Raab, M. Prentiss, A. Cable, S. Chu, and D. E. Pritchard, Phys. Rev. Lett. **59**(23), 2631 (1987).